Respiratory Research

RESEARCH

Open Access

Unraveling the role of HDAC3 as an immunotherapy prognostic biomarker and therapeutic target in advanced non-small cell lung cancer

Liyuan Dai[1], Liling Huang[1], Lin Li[2], Le Tang[1], Yuankai Shi[1*] and Xiaohong Han[3*]

Abstract

Background This study investigates HDAC3 as a potential immunotherapy biomarker in advanced non-small cell lung cancer (aNSCLC), focusing on its association with treatment response to immune checkpoint inhibitors (ICIs).

Methods We employed a multi-phase approach in 78 aNSCLC patients with 138 plasma samples, starting with a discovery phase that identified differential autoantibodies (AAbs) using proteomic analysis in responders and non-responders. In the validation phase, we assessed AAb levels at multiple time points. Additionally, immunohistochemistry and multiple immunofluorescence ($n=21$) were used to validate HDAC3 expression in FFPE samples, single-cell RNA sequencing ($n=26$) was performed to explore gene expression differences, cell and animal experiments were performed.

Results We identified 127 differential AAbs, with five key AAbs (HDAC3, METTL21C, HSPB3, SPACA7, and SPPL2B) consistently linked to prognosis pre- and post-treatment ($p<0.05$). A risk score model based on these AAbs effectively predicted progression-free survival. Furthermore, HDAC3 expression correlated with significant pathway enrichments and was associated with higher TGFβ1, PD-L1 infiltration and lower $CD8^+$ T cells infiltration ($p<0.05$). *HDAC3* knockdown significantly inhibited cell proliferation, impaired colony formation, and induced G0/G1 phase arrest in lung cancer cells. Preclinical models demonstrated that RGFP966, an HDAC3 inhibitor, combined with anti–PD-1 therapy enhanced $CD8^+$ T cell infiltration ($p<0.05$).

Conclusion Our findings underscore HDAC3's role as a biomarker for predicting ICI response in aNSCLC and suggest its potential as a therapeutic target, paving the way for future studies on HDAC3-targeted therapies to improve immunotherapy outcomes.

Clinical trial number not applicable.

Keywords HDAC3, Autoantibody, Immunotherapy, Prognostic biomarker, Non-small cell lung cancer

*Correspondence:
Yuankai Shi
syuankai@cicams.ac.cn
Xiaohong Han
hanxiaohong@pumch.cn

Full list of author information is available at the end of the article

Introduction

According to the 2020 GLOBOCAN report, lung cancer is the second most commonly diagnosed cancer worldwide, accounting for 11.4% of new cases, and it has the highest mortality rate, responsible for 18% of cancer-related deaths [1]. Non-small cell lung cancer (NSCLC) represents approximately 85% of these cases. Due to the lack of reliable screening tools and the often nonspecific early clinical symptoms, the majority of NSCLC patients are diagnosed at advanced stages, resulting in a poor prognosis [2–4]. Despite recent advances in treatment, particularly with the advent of immune checkpoint inhibitors (ICIs), the response to immunotherapy in aNSCLC patients remains highly variable, with non-responders constituting three-quarters of NSCLC patients under immunotherapy [5, 6], necessitating the identification of reliable prognostic biomarkers to guide clinical decisions and optimize therapeutic outcomes.

Histone deacetylase 3 (HDAC3) is a critical member of the histone deacetylase family, playing a pivotal role in epigenetic regulation by remodeling chromatin structure and influencing gene expression. Overexpression of HDAC3 has been implicated in various malignancies, contributing to tumor progression through mechanisms such as cell proliferation, apoptosis evasion, and metastasis [7–11]. Notably, HDAC3 has been associated with poor prognosis in lung cancer, serving as an independent predictor of survival outcomes [12]. Its involvement in tumor immunity further underscores its potential as a therapeutic target, as HDAC3 modulates immune responses by promoting $CD8^+$ T cell exhaustion and downregulating major histocompatibility complex class I expression on tumor cells [13–15].

Recent studies have demonstrated that inhibiting HDAC3 can restore T cell function and enhance the efficacy of immunotherapies in preclinical models [16–18]. The selective HDAC3 inhibitor RGFP966 has shown promise in reversing immune suppression in the tumor microenvironment, thereby improving the therapeutic effects of ICIs [16–18]. Given these findings, the present study aims to unravel the role of HDAC3 as a prognostic biomarker and a potential therapeutic target in aNSCLC, utilizing a comprehensive multi-phase approach that includes proteomic analysis, immunohistochemistry, single-cell RNA sequencing, and in vivo experiments. This investigation not only seeks to validate the prognostic significance of HDAC3 in aNSCLC but also aims to elucidate its mechanistic role in modulating the tumor immune microenvironment. The insights gained from this study could pave the way for novel therapeutic strategies that enhance the effectiveness of immunotherapy in patients with aNSCLC.

Methods

Study design and sample collection

This retrospective study aimed to explore HDAC3 as a potential immunotherapy biomarker in aNSCLC through a multi-phase approach. In the discovery phase ($n = 22$), proteomic analysis was used to identify differential AAbs between responders and non-responders to ICIs, revealing 127 AAbs—51 upregulated and 76 downregulated in non-responders. Considering the pivotal role of PD-L1 as a biomarker in lung cancer immunotherapy, an additional cohort ($n = 22$) with available PD-L1 expression data was analyzed to evaluate the independent predictive value of AAbs. This plasma cohort also underwent targeted protein microarray analysis.

Patients for both the discovery phase and validation phase were randomly selected to ensure unbiased sample representation. To ensure methodological rigor, the discovery cohort ($n = 22$) and validation cohort ($n = 34$) were designed with matched pre-treatment and post-treatment pairs. A balanced distribution of samples was maintained, with pretreatment samples (discovery: 22 vs. validation: 23) and post-treatment samples (discovery: 23 vs. validation: 25) allocated at a near 1:1 ratio. This is further supported by the absence of significant differences in clinical characteristics between cohorts, including gender distribution, ECOG, histology, and disease stage ($P > 0.05$). In the validation phase, we conducted aNSCLC-focused microarray analysis, comparing AAb levels in responders and non-responders at two time points. We identified 24 and 22 prognostic AAbs ($p < 0.05$), including five key AAbs (HDAC3, METTL21C, HSPB3, SPACA7, SPPL2B) with consistent expression patterns. We also performed a dynamic assessment in a cohort of patients at baseline and subsequent time points to track AAb trends, constructing a risk score model that predicted PFS. Additionally, HDAC3 expression was validated in 21 FFPE samples via immunohistochemistry and was associated with higher TGFβ1, PD-L1 infiltration and lower $CD8^+$ T cells infiltration, while single-cell RNA sequencing assessed gene expression differences between $HDAC3^+$ and $HDAC3^-$ cells, revealing significant pathway enrichments. Finally, we utilized si-HDAC3 and a C57BL/6 mouse model to evaluate the role of HDAC3 in lung cancer cells, the therapeutic effects of RGFP966 (an HDAC3 inhibitor) and anti–PD-1 antibodies on tumor growth and immune cell infiltration. This comprehensive approach aims to elucidate the role of HDAC3 in immune modulation and its potential as a biomarker for enhancing aNSCLC immunotherapy outcomes. Detailed clinical characteristics were shown in Tables S1 and S2.

Between 2016 and 2022, a total of 138 plasma samples were collected from 78 aNSCLC patients, including 67 pre-treatment samples (T0), 47 post-treatment samples (T1) within three months of ICIs therapy, 24

post-treatment samples (T2) at the time of three months. Additionally, 42 formalin-fixed paraffin-embedded (FFPE) samples were obtained from 42 aNSCLC patients who received ICI monotherapy (Nivolumab, Pembrolizumab, Sintilimab, or Tirellizumab) at the Cancer Hospital, Chinese Academy of Medical Sciences. All plasma samples were collected using ethylenediaminetetraacetic acid, centrifuged at 3000 rpm at 4 °C for 10 min, and stored in 2 ml conical tubes at -80 °C until the microarray assay. FFPE samples were stored at room temperature.

The inclusion criteria for patients were: (1) biopsy-confirmed aNSCLC with stage III or IV disease and with clinical data (gender, age, smoking history, ECOG, histological type, staging) and follow-up data (efficacy evaluation at 3 months and PFS); (2) treatment with ICI monotherapy; and (3) ICIs used as either first-line or later-line therapy. Patients were excluded if they met any of the following conditions: (1) a concurrent diagnosis of another cancer; (2) non-primary lung tumors; (3) concomitant autoimmune diseases; or (4) use of other immunosuppressive agents (e.g., steroid medication). The efficacy of immunotherapy was assessed using the Response Evaluation Criteria in Solid Tumours (RECIST) version 1.1. Patients were categorized as "responders" if they achieved complete remission, partial remission, or stable disease within three months of ICI treatment, and as "non-responders" if they experienced disease progression. This study was approved by the Ethics Committee of the National Cancer Center/National Clinical Research Center for Cancer/Cancer Hospital, Chinese Academy of Medical Sciences & Peking Union Medical College (No. 19–019/1804). All procedures were conducted in accordance with the principles of the Declaration of Helsinki.

HuProt™ microarray and aNSCLC-focused microarray

Standard experimental procedures for high-density microarrays have been described in our previous studies [19, 20]. Briefly, the HuProt™ microarray (CDI Labs, Mayaguez, PR) consisted of approximately 21,000 proteins. The microarray was retrieved from − 80 °C storage and blocked with bovine serum albumin (BSA, 9048-46-8, Sigma) for 1.5 h. Following the blocking step, the microarray was incubated with plasma samples at a 1:1000 dilution for 1 h. After washing with 0.1% phosphate-buffered saline-Tween 20, the plates were incubated with Alexa Fluor 647 goat anti-human IgG (109-605-003, Jackson) diluted in 5% BSA. The microarray was then scanned using a GenePix 4300 A microarray scanner (141095, Molecular Devices) with a 635 nm excitation laser. Signal intensities of IgG for each protein were quantified using GenePix Pro v.6.0 software (Molecular Devices). For the validation phase, candidate AAbs identified during the discovery phase were selected and printed onto 2 × 7 sub-arrays to create an aNSCLC-focused microarray. The experimental procedures for the aNSCLC-focused microarray were similar to those used for the high-density microarray, except for the blocking and dilution buffer, which was 3% BSA.

Immunohistochemistry validation

All patient samples underwent hematoxylin-eosin staining and were meticulously reviewed by two experienced pathologists to identify cancer lesions. Immunohistochemistry (IHC) was performed on FFPE samples following dewaxing and heat-induced antigen retrieval. After washing, the samples were treated with a 3% hydrogen peroxide solution to quench endogenous peroxidase activity. Primary antibodies, including rabbit anti-human IgG antibodies specific to histone deacetylase 3 (HDAC3, ab32369, Abcam), were applied at a 1:500 dilution following blocking with rabbit serum. After incubation, the samples were treated with a 1:200 dilution of HRP-labeled goat anti-rabbit IgG secondary antibody (GB23303, Servicebio) for 50 min at room temperature. Diaminobenzidine (DAB) was used for color development, and the nuclei were counterstained with hematoxylin (G1004, Servicebio). The results were examined under a white light microscope (E100, Nikon) and quantified using CaseViewer 2.4 (3DHISTECH, Hungary) software. Protein expression levels were quantified using an H-score, which was calculated based on the intensity of the stain and the percentage of positive tumor cells, with scores ranging from 0 to 300. Staining intensity was categorized as negative (0), weak (1), moderate (2), or strong (3), and the percentage of positive cells was scored from 0 to 100. The H-score was determined by multiplying the intensity score by the percentage of positive cells. An H-score below 60 was classified as low expression, while an H-score of 60 or above was considered high expression.

Single-cell and bulk-RNA sequencing analysis of HDAC3

Data from GSE131907 ($n = 21$), which includes NSCLC tumor samples (including advanced stage lung tumors, lymph node metastases, and brain metastases), as well as data from GSE182434 ($n = 5$), consisting of four tumor samples from DLBCL and one tonsil sample from a patient with tonsillitis, were retrieved. Clinical data and metadata were obtained from the original study [21, 22]. Additionally, immunotherapy-related dataset GSE218989 [23] ($n = 339$ NSCLC) was annotated and utilized for immunotherapy prediction analysis. Raw data underwent rigorous quality control using the "Affy" package [24] within R software, involving the computation of average values for multiple probes corresponding to a single gene. The risk score was calculated using the formula: risk score = Σ (Expression * Coefficient) and generated through the use of the "ggrisk" package.

Initially, quality control was performed on the GSE131907 data using "Seurat" [25] package, which focused on single-cell RNA-seq data analysis, particularly for clustering and dimensionality reduction. Using Seurat, we were able to perform quality control, normalization, and integration of datasets, followed by clustering cells based on gene expression profiles. Quality control was focusing on cell quality by filtering based on the number of detected genes (minimum: 300, maximum: 6000), mitochondrial gene percentage (0–15%), hemoglobin gene percentage (0–0.1%), and ribosomal gene percentage (minimum: 1–100%). Genes expressed in fewer than three cells were excluded. Malignant epithelial cells were then isolated. Based on the expression status of *HDAC3*, these malignant epithelial cells were classified into '*HDAC3*-positive' and '*HDAC3*-negative' groups. Copy number variations (CNVs) analysis was subsequently conducted on these cells using the "inferCNV" [26] package, which was applied to detect CNVs from single-cell RNA-seq data, calculating CNV scores for each cell type. By analyzing the expression levels of genes across cells, inferCNV allowed us to infer CNVs that could distinguish cancerous from non-cancerous cells, providing insights into the genomic landscape of the tumors. Additionally, "GSEABase" [27] package was used to perform rank-based Gene Set Enrichment Analysis (GSEA). It provided the tools to access, organize, and work with gene sets, allowing us to evaluate whether specific pathways or biological processes were significantly enriched in our data, helping to interpret the functional implications of gene expression changes in the context of cancer.

To investigate the differences in interactions between *HDAC3*$^+$ and *HDAC3*$^-$ tumor cells and immune cells (including exhausted Tfh, exhausted CD8$^+$ T cells, cytotoxic CD8$^+$ T cells, CD8$^+$/CD4$^+$ mixed Tfh, CD8$^+$ low T cells, CD4$^+$ Tfh, NK cells, naive CD8$^+$ T cells, naive CD4$^+$ T cells, and microglia / macrophage cells), the "CellChat" [28, 29] package was employed to analyze cell-cell communication. It facilitated the identification of signaling pathways involved in tumor-immune cell interactions. By constructing cell-cell communication networks, we could explore the potential roles of specific ligand-receptor pairs in mediating immune responses in the tumor microenvironment. Specific categories within the CellChat database, such as "Secreted Signaling," "ECM-Receptor," and "Cell-Cell Contact," were examined, with a minimum cell count criterion of three applied.

Multiple Immunofluorescence

FFPE tissue sections of 4–5 μm thickness were prepared, followed by dewaxing and rehydration. Antigen retrieval was performed, and endogenous peroxidase activity was blocked using an antibody blocking solution. Sequential immunostaining was carried out for each target antigen, including primary antibodies against rabbit anti-human IgG for HDAC3 (ab32369, 1:250, Abcam), CD8A (ab237709, 1:500, Abcam), TGFB1 (ab215715, 1:500, Abcam), PD-L1 (#13684S, 1:800, CST), and mouse anti-human pan cytokeratin IgG (ab7753, 1:250, Abcam). This was followed by incubation with secondary antibodies: HRP-labeled goat anti-rabbit IgG (GB23303, 1:500, Servicebio) for HDAC3, CD8A, and TGFB1 and HRP-labeled goat anti-mouse IgG (GB23301, 1:500, Servicebio) for pan cytokeratin. Tyramide signal amplification (TSA) was employed, followed by microwave treatment to remove the TSA-antibody complex, allowing for subsequent rounds of antibody labeling. After immunostaining, cell nuclei were counterstained with 4',6-diamidino-2-phenylindole, and slides were coverslipped for scanning. Microscopy (ECLIPSE C1, Nikon) and scanning (Pannoramic MIDI, 3DHISTECH) were used for result interpretation. The CaseViewer 2.4 (3DHISTECH) and ImageJ software were utilized to quantify the number and percentage of positive cells. All results were independently reviewed by two experienced pathologists.

Cell and animal experiment

Cell culture and transfection

Human non-small cell lung cancer cell lines A549 and H1299 were obtained from the American Type Culture Collection (ATCC). Cells were cultured in RPMI-1640 medium (Gibco, USA) supplemented with 10% fetal bovine serum (FBS, Gibco, USA) and 1% penicillin/streptomycin (Gibco, USA) at 37 °C in a humidified atmosphere containing 5% CO_2. Cells were passaged when they reached 70–80% confluence. The Lewis (catalog KG070) mouse lung cancer cell line was cultured in DMEM supplemented with 10% fetal bovine serum at 37 °C and 5% carbon dioxide. All experiments were conducted using mycoplasma-free cells.

RNA interference and lentiviral infection

To construct the RNA interference (RNAi) vector targeting *HDAC3*, single-stranded DNA oligonucleotides with the interference sequences were synthesized. These oligonucleotides were annealed to form double-stranded DNA and ligated into the pre-digested RNAi vector. The ligation products were transformed into competent bacteria, and correct clones were confirmed by sequencing.

Lentiviral vectors expressing *HDAC3* shRNA were generated by co-transfecting HEK-293T cells with the RNAi plasmid and packaging plasmids using Lipofectamine 2000 (Invitrogen, USA). After 48 h, the culture supernatant was collected, filtered, and concentrated to obtain the lentivirus. A549 and H1299 cells were infected with the concentrated lentivirus for *HDAC3* knockdown.

Stable clones were selected by incubation with puromycin (1 μg/mL, Sigma-Aldrich, USA) for 2 weeks. Successful knockdown of *HDAC3* was confirmed by qPCR and Western blot analysis.

For qPCR, specific primers for the target genes (*HDAC3* and *GAPDH*) were designed using Primer3 software based on the gene sequences obtained from the GenBank database. The primers used for qPCR are as follows: *HDAC3*_Forward (CGCTATGTGGATACGCTGCTTTA), *HDAC3*_Reverse (GCAACCAGGATTTATACAAGGAGGA), *GAPDH*_Forward (GTCTCCTCTGACTTCAACAGCG), and *GAPDH*_Reverse (ACCACCCTGTTGCTGTAGCCAA). For Western blot, The primary antibodies used were Anti-β-Actin (1:1000, CST, #4970S) and Anti-HDAC3 (1:5000, Abcam, ab32369).

Cell proliferation assays (CCK-8)

Cell proliferation was assessed using the CCK-8 assay (Dojindo, Japan). A549 and H1299 cells were seeded in 96-well plates and allowed to adhere overnight. Cells were transfected with *HDAC3*-targeting shRNA or control vectors as described above. At 24, 48, and 72 h post-transfection, CCK-8 reagent (10 μL) was added to each well, and the cells were incubated for 2 h at 37 °C. Absorbance was measured at 450 nm using a microplate reader. The proliferation rate was calculated relative to the control group.

Colony formation assay

For the colony formation assay, cells in the logarithmic growth phase were trypsinized with 0.25% trypsin and dissociated into a single-cell suspension by pipetting. The cell suspension was resuspended in complete culture medium. The cell suspension was then serially diluted and seeded in 6-well plates at a density of approximately 300 cells per well. Cells were evenly distributed and allowed to settle for 2–3 weeks in the incubator, with medium replacement every 4–5 days. Once visible colonies appeared, culture was terminated. The medium was discarded, and cells were carefully washed twice with PBS. Cells were then fixed with 1 mL of 4% paraformaldehyde for 15 min, followed by staining with crystal violet solution for 20 min. The staining solution was gently washed off with deionized water, and the colonies were allowed to air dry. Colonies were counted and photographed.

Cell cycle analysis

Cell cycle distribution was analyzed by flow cytometry. A549 and H1299 cells were transfected with *HDAC3*-targeting shRNA or control vectors, and at 48 h post-transfection, cells were harvested, washed with cold PBS, and fixed in 70% ethanol at 4 °C overnight. Fixed cells were then stained with propidium iodide (PI) solution containing RNase A for 30 min at 37 °C.

Animal experiment

RGFP966 is a specific inhibitor of HDAC3, N-(o-aminophenyl)carboxamide, purchased from MedChemExpress (catalog HY-13909) [30, 31]. Male C57BL/6 mice (6–8 weeks old) were sourced from Shanghai GemPharmatech. These mice were housed in a specific pathogen-free animal facility with free access to food and water. They were maintained at 22 °C ± 2 °C with a relative humidity of 70%, under a 12-hour light/dark cycle. To establish the NSCLC model, Lewis (1 × 10^7) cells were injected into the flanks of C57BL/6 mice. Tumors were monitored and measured with calipers every 2–3 days. After 8 days of Lewis cell implantation, tumor volumes reached approximately 100 mm^3. C57BL/6 mice carrying Lewis cells were randomly divided into three groups ($n = 3$), including a control group, an anti-PD-1 mAb group, and an RGFP966 plus mAb anti-PD-1 group. RGFP966 (catalog HY-N0504) was dissolved in PBS and administered to mice at a dosage of 25 mg/kg daily. The PD-1 monoclonal antibody (catalog BE0146, BioXCell) was dissolved in PBS and intravenously administered at a dose of 200 μg three times a week. The control group received only intravenous PBS. Treatment continued until tumor volume exceeds 3000 mm^3. Mice were euthanized with an overdose of 0.5% pentobarbital sodium, and tumors were excised, photographed, and weighed. The resected tumors were subjected to flow cytometry analysis.

Statistical analysis

All statistical analyses were conducted using IBM SPSS Statistics 24 (Chicago,

Illinois, USA), R version 4.2.1, Sanger plot (http://www.sangerbox.com), and Hiplot (https://hiplot.com.cn/home/index.html). The Mann-Whitney U test was used for group comparisons. Sensitivity, specificity, and ROC curves were calculated using the "pROC" [32] and "ROCR" [33] packages in R. The "maxstat" [34] package in R was employed to determine the optimal cutoff values for categorizing high- and low-expression groups for survival analysis in both the discovery and validation phases. A p-value of < 0.05 (two-tailed) was considered statistically significant for all analyses.

Results

aNSCLC AAbs validation in aNSCLC-focused microarray

Our previous study [19] identified 127 differential AAbs between responders and non-responders that overlapped in the pre- and on-ICIs monotherapy in the discovery phase, as shown in Table S3, with 51 AAbs elevated and 76 AAbs decreased in non-responder group. To address concerns regarding the randomization of the discovery

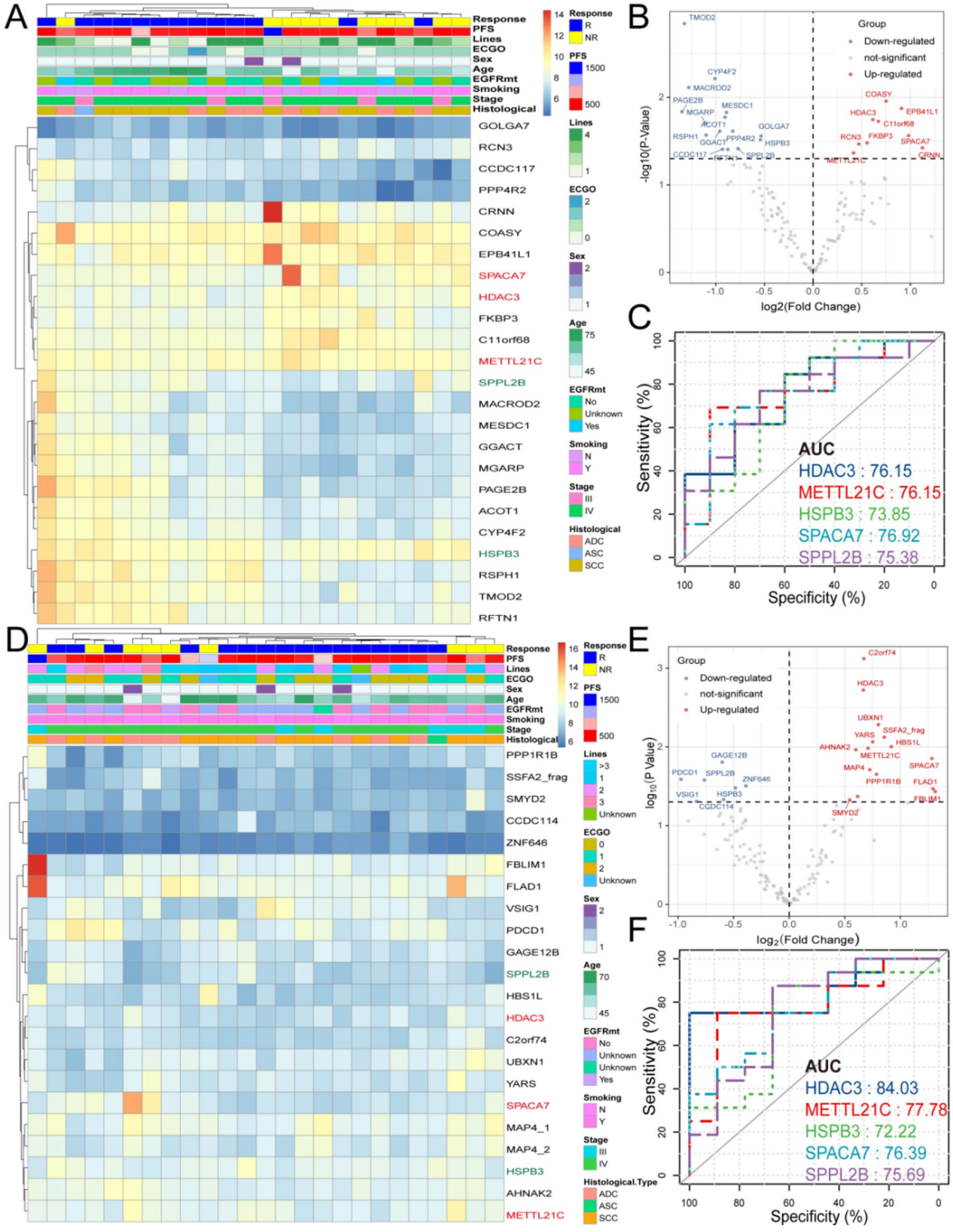

Fig. 1 (See legend on next page.)

(See figure on previous page.)

Fig. 1 Validation of differential AAbs using high-density microarrays pre- ($n=23$) and on-ICIs monotherapy ($n=25$) ($p<0.05$). **A**, **D**. Heatmaps illustrating differential AAbs between responders and non-responders pre- and on-ICIs monotherapy, based on normalized intensity data (Z-Scored across individuals and $p<0.05$). **B**, **E**. Volcano plots displaying differential AAbs between responders and non-responders pre- and on-ICIs monotherapy based on the normalized intensity data (Z-Scored across individuals and $p<0.05$). **D**, **F**. ROC curves of the five overlapping AAbs (HDAC3, METTL21C, HSPB3, SPACA7, and SPPL2B) predicting responder and non-responder patients pre- and on-ICIs monotherapy. (*Abbreviation: AAb: autoantibody; ICIs: immune checkpoint inhibitors; ROC: receiver operating characteristic.*)

and validation cohorts, we conducted a sensitivity analysis for HDAC3 autoantibodies. For the pre-treatment cohort of 45 patients, we performed 100 random splits into two nearly equal groups (22 vs. 23 patients). In 85% of these splits, the hazard ratios (*HR*s) remained consistent in the same direction ($HR>1$) (Figure S1A). Similarly, for the post-treatment cohort of 47 patients, 95% of the 100 random splits showed consistent *HR* directions ($HR>1$) (Figure S1B). These results confirm that our findings are robust and not dependent on the specific cohort division, further supporting the stability and generalizability of our conclusions. In the aNSCLC-focused microarray validation phase, we compared responders ($n=13$) and non-responders ($n=10$) at T0 and T1 time points using normalized intensity data. A total of 24 AAbs and 22 AAbs ($p<0.05$) were identified as prognostic AAbs (Fig. 1). Among these, five AAbs (HDAC3, METTL21C, HSPB3, SPACA7, and SPPL2B) were consistently detected in both the pre- and on-ICIs monotherapy, with areas under the curve (AUCs) of 0.76, 0.76, 0.74, 0.77, and 0.75 in the pre-ICIs monotherapy (Fig. 1A-C) and 0.84, 0.78, 0.72, 0.76, and 0.76 in the on-ICIs monotherapy (Fig. 1D-F). All five AAbs showed differential expression between the pre- and on-ICIs monotherapy, with SPACA7, HDAC3, and METTL21C being higher ($p<0.05$) in the non-responder group, while HSPB3 and SPPL2B were higher ($p<0.05$) in the responder group (Fig. 2A-B). Considering that patients with *EGFR*-mutant lung cancer have poorer responses to immunotherapy compared to those with *EGFR* wild-type, we compared the levels of HDAC3 autoantibody intensity among three groups: *EGFR*-mutant, *EGFR* wild-type, and unknown *EGFR* status. We also analyzed whether HDAC3 autoantibody independently predicts PFS regardless of *EGFR* mutation status. The results showed no significant differences in HDAC3 autoantibody levels among the three groups ($P>0.05$) (Fig. S2A), while HDAC3 autoantibody was an independent prognostic predictor of PFS ($P<0.05$) (Figure S2B).

In the dynamic cohort, these five AAbs were evaluated at baseline ($n=15$), 1 month ($n=14$), 1.5 months ($n=14$), and 3 months ($n=10$). HDAC3 AAb showed higher levels in non-responders compared to responders at baseline and 3 months ($P<0.05$). HSPB3 AAb showed higher levels in responders compared to non-responders at baseline ($P<0.05$), while METTL21C AAb showed higher levels in non-responders compared to responders at baseline ($P<0.05$). SPPL2B AAb showed higher levels in non-responders compared to responders at baseline, 1 month, and 3 months ($P<0.05$). Although SPACA7 AAb levels consistently trended higher in responders across all timepoints, these differences did not reach statistical significance (Fig. 2C). A risk score model based on these five AAbs was constructed for both pre- and on-ICIs monotherapy, with the risk score calculated as: risk score = Σ (Expression * Coefficient) (Fig. 3A). High-risk score groups were associated with poorer PFS in both pre- and on-ICIs monotherapy ($p<0.05$) (Fig. 3A). These five AAbs demonstrated correlations with laboratory tests: HDAC3 AAb was associated with MCV, BASO, and IgA, while METTL21C AAb and SPACA7 AAb correlated with CEA and ALP (Fig. 3B). Patients with liver metastasis exhibited significantly higher levels of HDAC3 and CRNN AAbs ($p<0.05$), whereas patients with lung metastasis showed elevated levels of HSPB3 and METTL21C AAbs ($p<0.05$) (Fig. 3C). Additionally, *HDAC3* was identified as a prognostic marker for PFS ($p<0.01$) (Fig. 3D) in GSE218989, which containing 339 NSCLC patients receiving ICIs therapy. PD-L1 expression was not predictive of PFS, regardless of the stratification method—whether dichotomized (TPS < 50% vs. TPS ≥ 50%) or divided into three categories (TPS < 1%, TPS = 1–50%, and TPS ≥ 50%) ($P>0.05$) (Fig. 3E). In contrast, HDAC3 AAbs demonstrated prognostic value among the 22 patients with available PD-L1 expression data, showing a positive correlation with PD-L1 levels; patients with higher HDAC3 AAb levels tended to exhibit higher PD-L1 expression ($P<0.05$) (Fig. 3F).

Validation of HDAC3 in IHC, scRNA-seq, and mIF cohorts

HDAC3 protein expression was assessed in 21 NSCLC FFPE samples. Representative examples of HDAC3 expression, ranging from negative, weak, moderate to strong were shown in Fig. 3G. IHC staining of HDAC3 in two representative patients with different PFS was illustrated in Fig. 3G (patient 1 with a long PFS of 24.9 months, stage III, and patient 2 with a short PFS of 2.67 months, stage III). HDAC3 protein expression demonstrated predictive value for PFS ($p<0.05$) (Fig. 3G). Two overlapping patients in the autoantibody and IHC cohorts showed that patients with high expression of HDAC3 protein also had high levels of HDAC3 autoantibodies (Fig. 3H).

HDAC3$^+$ malignant lung cancer cells exhibited significantly higher expression of *UBE2S*, *PPP1R14B*, *EGFR1*, *AREG*, *CHI3L1*, *BRI3*, *CXCL2*, *SOD3*, *SLC25A6*, *TGM2*, *VIM*, *ISG15*, *MUC5B*, *CTSE*, *FAM177A1*, *CD74*, *RPS4Y1*, and *NFKBIA* ($p < 0.05$) and lower expression of *AKR1B1*, *MT1X*, *PIGR*, *UBC*, *HILPDA*, *HMGB3*, *HSPA1B*, *ARGLU1*, *HNRNPH1*, *MGP*, *SAA1*, *N4BP2L2*, *HIST1H10*, *POLR2J3*, *KCNQ1OT1*, *SCGB3*, *RPS4Y1*, *MALAT1*, *HSPA6*, *WSB1*, and *SFTPA2* ($p < 0.05$) compared to *HDAC3*- malignant lung cancer cells in GSE131907 (Fig. 4A). *HDAC3*$^+$ cells showed significant enrichment in ($p < 0.001$) NRF2, IL-17, and NF-kappa B signaling pathways (Fig. 4B). Furthermore, *HDAC3*$^+$ malignant lung cancer cells exhibited higher chromosomal copy number variation (CNV) scores ($p < 0.001$) compared to *HDAC3*$^-$ malignant lung cancer cells (Fig. 4C). Enrichment analysis of *HDAC3*$^+$ cells revealed significant associations with pathways including the unfolded protein response, reactive oxygen species pathway, protein secretion, PI3K-AKT-MTOR, P53, oxidative phosphorylation, Myc targets, MTORC1, adipogenesis, and DNA repair signaling ($p < 0.05$) (Fig. 4D). *HDAC3*$^+$ malignant lung cancer cells also had significantly higher epithelial-mesenchymal transition (EMT) scores than HDAC3$^-$ cells ($p < 0.001$) (Fig. 4D).

Analysis of interactions between *HDAC3*$^+$ tumor cells and immune cells, as well as *HDAC3*$^-$ tumor cells and immune cells (including exhausted T follicular helper (Tfh) cells, exhausted CD8$^+$ T cells, cytotoxic CD8$^+$ T cells, CD8$^+$/CD4$^+$ mixed Tfh cells, CD8$^+$ low T cells, CD4$^+$ Tfh cells, NK cells, naive CD8$^+$ T cells, naive CD4$^+$ T cells, and microglia/macrophage cells), showed that *HDAC3*$^+$ tumor cells interact more closely with immune cells than *HDAC3*$^-$ cells. This includes interactions with exhausted and cytotoxic CD8$^+$ T cells, CD4$^+$ Tfh cells, NK cells, and macrophages (Fig. 5A). Specific interactions, such as TGFB1-ACVR1B/TGFBR2, were unique to *HDAC3*$^+$ cells and immune cells (Fig. 5B). In malignant lung tumors, *HDAC3* expression positively correlated with *TGFB1* ($R = 0.72$), *TGFBR2* ($R = 0.68$), and *ACVR1B* ($R = 0.62$) ($p < 2.2e\text{-}16$) (Fig. 5C). In the mIF cohort, samples with higher levels of HDAC3$^+$ tumor cells exhibited higherTGFβ1 infiltration ($p < 0.05$, $R = 0.49$) (Fig. 5D). The intensity of HDAC3$^+$ tumor cells was found to have predictive value for OS ($p < 0.01$) (Fig. 5E). Furthermore, the percentage of TGFβ1 infiltration was significantly higher in patients with increased HDAC3$^+$ tumor cells ($p < 0.05$) (Fig. 5E). HDAC3 intensity showed a positive correlation with PD-L1 intensity in aNSCLC patients ($p < 0.05$, $R = 0.45$) (Fig. 5F). Representative mIF staining of HDAC3$^+$ tumor cells, CD8$^+$ T cells, PD-L1, and TGFβ1 infiltration was shown for a patient with a short OS of 48 days compared to a patient with a long OS of 894 days Fig. 5G. Given the extensive studies [18, 35, 36] on HDAC3 in lymphoma, we also investigated the expression of HDAC3 in a single-cell DLBCL cohort (GSE182434) [22]. This analysis was motivated by previous findings demonstrating the significant role of HDAC3 inhibition in modulating tumor immune responses and epigenetic programming in DLBCL. Based on our prior study on DLBCL [37], malignant B cells in GSE182434 were categorized into low and high malignancy groups. *HDAC3* expression was found to be higher in high-malignancy B cells (Figure S3A).

HDAC3 inhibitor shapes tumor microenvironment in lung cancer

To investigate the effects of HDAC3 on lung cancer cells, we performed *HDAC3* knockdown in A549 and H1299 cell lines. mRNA and protein level analysis confirmed that siRNA effectively inhibited *HDAC3* expression (Figure S3B-C). Cell proliferation assays showed a significant decrease in cell proliferation following *HDAC3* knockdown (Figure S4A), and colony formation ability was also significantly impaired (Figure S4B). Flow cytometry analysis revealed that *HDAC3* knockdown induced cell cycle arrest at the G0/G1 phase (Figure S4C). These results suggest that HDAC3 plays a crucial role in the proliferation of lung cancer cells.

Given that higher levels of HDAC3$^+$ tumors were associated with lower infiltration of CD8$^+$ T cells, we hypothesized that the use of HDAC3 inhibitors could enhance the therapeutic efficacy of anti–PD-1 immunotherapy. We administered RGFP966 and/or anti–PD-1 antibodies to C57BL/6 mice harboring Lewis cells (Fig. 6A). Both monotherapy and combination therapy did not affect the weight of the mice (Fig. 6B), indicating good tolerance. Treatment with either the combined therapy or anti–PD-1 therapy resulted in a significant decrease in both tumor volume (Fig. 6B) and tumor weight (Fig. 6C) ($p < 0.05$). Flow cytometry analysis revealed that the combined therapy significantly increased CD3$^+$ CD8$^+$ cell infiltration ($p < 0.05$), while anti–PD-1 immunotherapy was not (Fig. 6C). In summary, these findings suggest that inhibition of HDAC3 may reshape the inflamed tumor microenvironment in vivo.

Discussion

This study investigates HDAC3 as a potential immunotherapy biomarker in aNSCLC, revealing its significant association with treatment responses to ICIs and patient outcomes. Employing a multi-phase approach, we identified and validated several AAbs linked to PFS. In the discovery phase, we identified 127 differential AAbs between responders and non-responders, and the validation phase confirmed 24 and 22 prognostic AAbs at different time points through microarray analysis. Notably, five key AAbs (HDAC3, METTL21C, HSPB3, SPACA7,

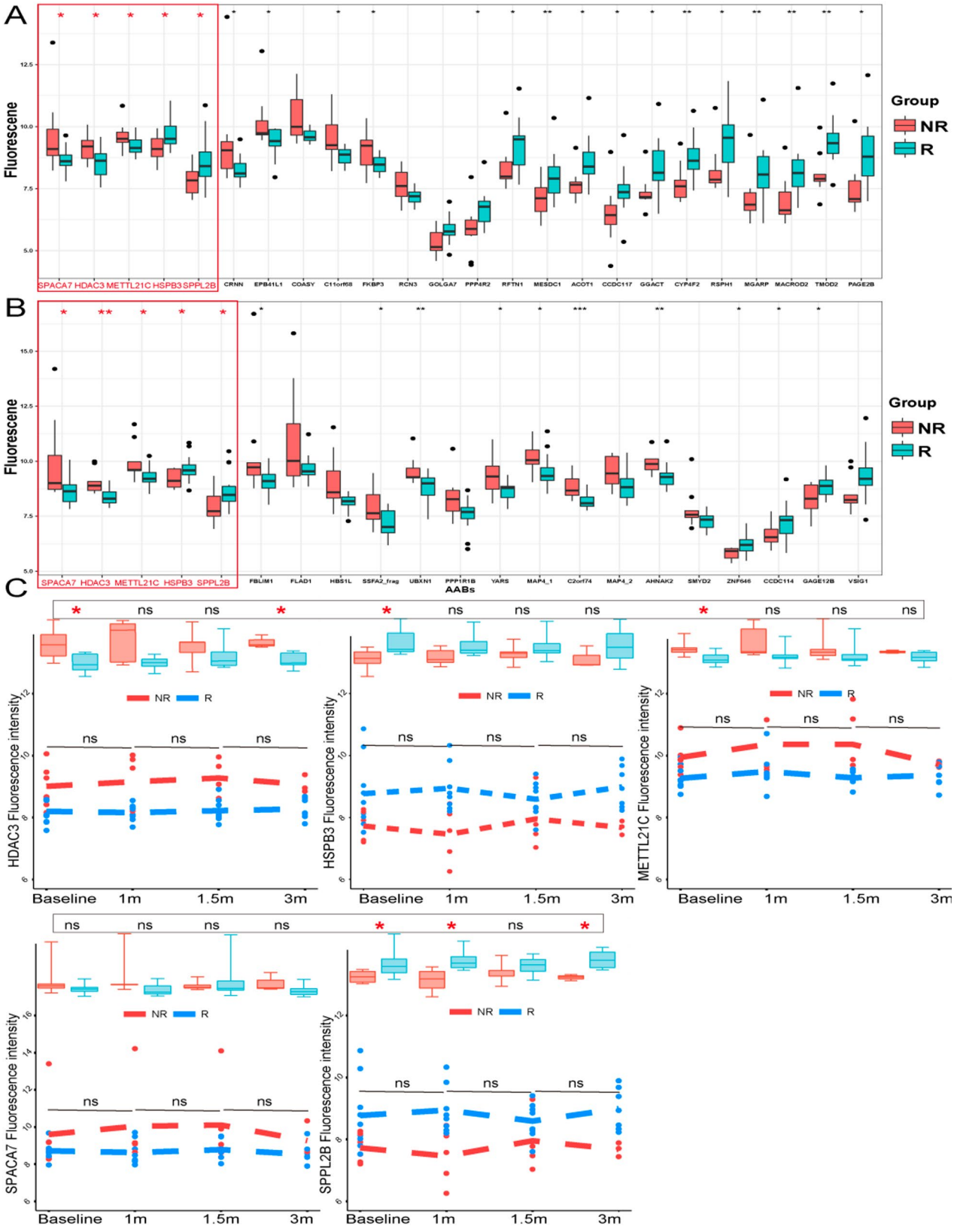

Fig. 2 Differential and dynamic analyses of AAbs pre- and on-ICIs monotherapy. **A**-**B**. Comparison of prognostic AAbs ($p < 0.05$) between responders and non-responders pre- ($n = 24$) and on-ICIs monotherapy ($n = 22$). **C**. Dynamic changes in five AAbs (HDAC3, METTL21C, HSPB3, SPACA7, and SPPL2B) at baseline, 1 month, 1.5 months, and 3 months pre- and on-ICIs monotherapy. (Abbreviation: AAb: autoantibody; ICIs: immune checkpoint inhibitors. * $p < 0.05$, ns: not significant.)

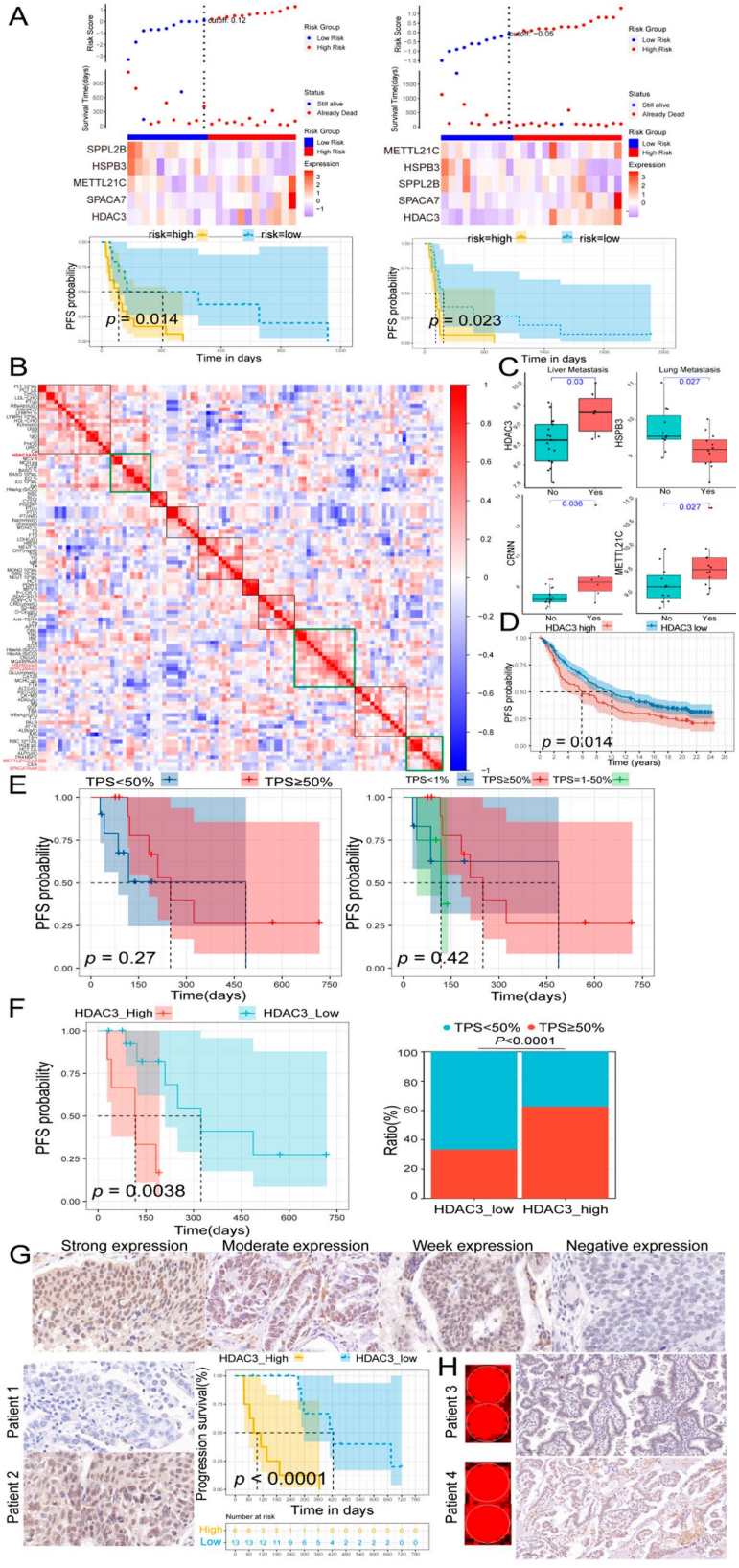

Fig. 3 (See legend on next page.)

(See figure on previous page.)

Fig. 3 Performance of the five AAbs risk score model in predicting PFS pre- and on-ICIs monotherapy and its correlation with clinical factors and prognostic value of HDAC3 AAb ($n = 22$) and HDAC3 protein in IHC cohort ($n = 21$, 100X). **A**. Scatter plots, heatmaps, and Kaplan-Meier curves showing PFS in high-risk versus low-risk score groups pre- and on-ICIs monotherapy. **B**-**C**. Heatmap and box plots depicting the correlation between differential AAbs and clinical factors. **D**. Kaplan-Meier curves for PFS based on *HDAC3* mRNA expression in the GSE218989 dataset. **E**. Kaplan-Meier curve for PFS based on PD-L1 expression (group 1: TPS < 50% and TPS ≥ 50%; group 2: TPS < 1%, TPS = 1–50%, and TPS ≥ 50%). **F**. Kaplan-Meier curve for PFS based on HDAC3 AAb and the correlation of PD-L1 and HDAC3 AAb. **G**. Representative IHC staining images showing HDAC3 expression levels from strong to moderate, weak, and negative; patient 1 (PFS = 24.9 months) and patient 2 (PFS = 2.67 months) are depicted, along with Kaplan-Meier survival curves for PFS grouped by HDAC3 expression levels. **H**. The levels of HDAC3 autoantibodies and HDAC3 protein expression in two patients (Patient 3: PFS = 718 days and patient 4: PFS = 365 days) with overlapping autoantibody and IHC cohorts. (*Abbreviation: AAb: autoantibody; PFS: progression-free survival; ICIs: immune checkpoint inhibitors; IHC: immunohistochemistry.*)

and SPPL2B) exhibited consistent expression patterns, underscoring their dynamic nature during pre-treatment and on-treatment phases. Furthermore, IHC validation of HDAC3 confirms its prognostic value, correlating with PFS. Single-cell RNA sequencing reveals significant pathway enrichments in $HDAC3^+$ malignant cells, indicating its role in immune modulation. Notably, $HDAC3^+$ tumor cells show higher TGFβ1 infiltration and lower $CD8^+$ T cell infiltration, emphasizing the therapeutic potential of targeting HDAC3 to enhance immune responses in the mIF cohort. Our preclinical model demonstrates that RGFP966, an HDAC3 inhibitor, in combination with anti–PD-1 therapy, improves $CD8^+$ T cell infiltration, suggesting that HDAC3 inhibition may enhance the efficacy of immunotherapy.

Histone deacetylase 3 (HDAC3) is a key member of the histone deacetylase family, primarily regulating gene expression by remodeling chromatin and playing a crucial role in epigenetics [38–40]. The functions of HDAC3 include several major aspects: (1) promoting cell proliferation and participating in cell cycle regulation. HDAC3 is overexpressed in various malignant tumors, particularly in processes such as tumor proliferation, apoptosis, metastasis, angiogenesis, and cancer drug resistance [9]. In colorectal cancer, the deletion of HDAC3 inhibits cell proliferation, invasion, and migration by reducing the expression of TGIF1, thereby slowing tumor growth and inducing cell apoptosis [8]. In endometrial cancer, inhibiting HDAC3 increases STRING expression, thereby suppressing tumorigenesis [10]. In gastric cancer, overexpression of HDAC3 is associated with poor prognosis [11]. Furthermore, HDAC3 plays a critical role in cancer stem cells through genome-wide epigenetic modifications [41, 42]. In lung cancer, high expression of HDAC3 is considered an independent prognostic factor for patients with lung adenocarcinoma [12] and is also highly expressed in brain metastatic lung adenocarcinoma [43]. The absence of HDAC3 expression disrupts the expression of Wnt ligands, leading to reduced Wnt activity [44]. Inhibition of HDAC3 helps NSCLC overcome osimertinib resistance [45]. (2) Regulation of PD-L1 expression. The regulatory mechanism of HDAC3 on PD-L1 exhibit dual roles depending on the immune context and cancer subtype. In lymphoma [36], melanoma [46], and gastric cancer [47], HDAC3 functions as a negative regulator of PD-L1, whereas in pancreatic cancer [16] and thymic epithelial tumors [48], HDAC3 positively regulates PD-L1 expression. In lymphoma [36], HDAC3 inhibitors (HDAC3i) can rapidly increase histone acetylation in the *PD-L1* gene promoter region and recruit bromodomain protein BRD4, thus activating transcription. In melanoma, HDAC3 interacts with RORA and participates in the RORA-mediated suppression of PD-L1 [46]. In pancreatic cancer [16], the selective HDAC3 inhibitor RGFP966 can reduce both the protein and mRNA levels of PD-L1 in pancreatic cancer cells. (3) Regulation of genes such as TGF-β1 and promotion of $CD8^+$ T cell exhaustion. In tumor immunotherapy, HDAC3 can inhibit the expression of cytotoxic genes through histone acetylation modifications, promoting $CD8^+$ T cell exhaustion [13, 15]. Inhibiting HDAC3 can enhance chemotaxis and immune cell recruitment mediated by CXCL10, promoting anti-tumor immunity [49]. Consistent with our research findings, high expression of HDAC3 and its own antibodies is positively correlated with poor PFS and OS in NSCLC patients. Our experiments demonstrate that HDAC3 not only regulates the proliferation of lung cancer cells, PD-L1 expression, and TGFB1 expression, but also modulates $CD8^+$ T cell infiltration in vivo.

The advantages of existing preclinical and clinical HDAC3 inhibitors include: (1) Cell specificity: HDAC inhibitors can specifically inhibit HDAC activity in tumor cells with relatively low toxicity to normal cells, offering better safety and tolerance; (2) Multi-target effects: HDAC inhibitors act on multiple targets in tumor cells, including cell proliferation and cell cycle regulation, providing a more comprehensive therapeutic effect; (3) Combination with immunotherapy: HDAC3i can lower DNMT1 protein levels, indirectly activating PD-L1 transcription. Combined use of CTLA-4 and PD-1 antibodies can lead to upregulation of PD-L1 on early tumor antigen-presenting cells and expression of PD-1 on tumor-infiltrating effector T cells. In mouse models of melanoma and breast cancer [50, 51], HDACi induces rapid acetylation of PD-L1 genomic histones, triggering persistent gene expression, significantly enhancing the in vivo PD-1/CTLA-4 blocking response. Compared

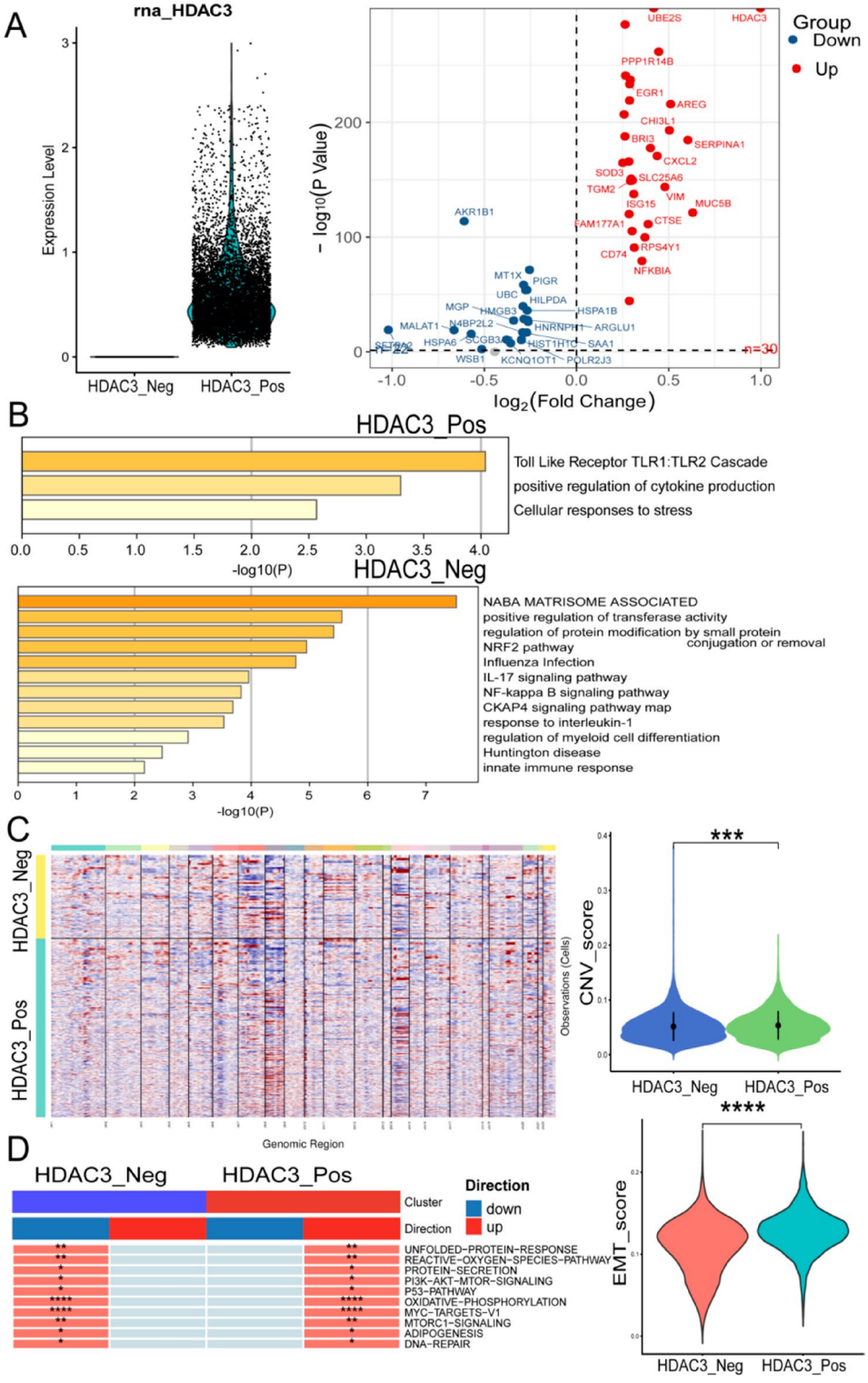

Fig. 4 Aanysis of *HDAC3*$^{+}$ and *HDAC3*- tumor cells in NSCLC using single-cell RNA sequencing in GSE131907. **A**. Volcano plots displaying differential gene expression between *HDAC3*$^{+}$ and *HDAC3*$^{-}$ tumor cells. **B**. Functional enrichment analysis of differential expressed genes. **C**. Heatmap and comparison of CNV scores between *HDAC3*$^{+}$ malignant cells and *HDAC3*$^{-}$ malignant cells. **D**. GSEA of hallmark pathways and comparison of EMT scores between *HDAC3*$^{+}$ and *HDAC3*$^{-}$ tumor cells. (Abbreviation: NSCLC: non-small cell lung cancer; CNV: copy number variation; EMT: epithelial–mesenchymal transition. *** $p < 0.001$,**** $p < 0.0001$.)

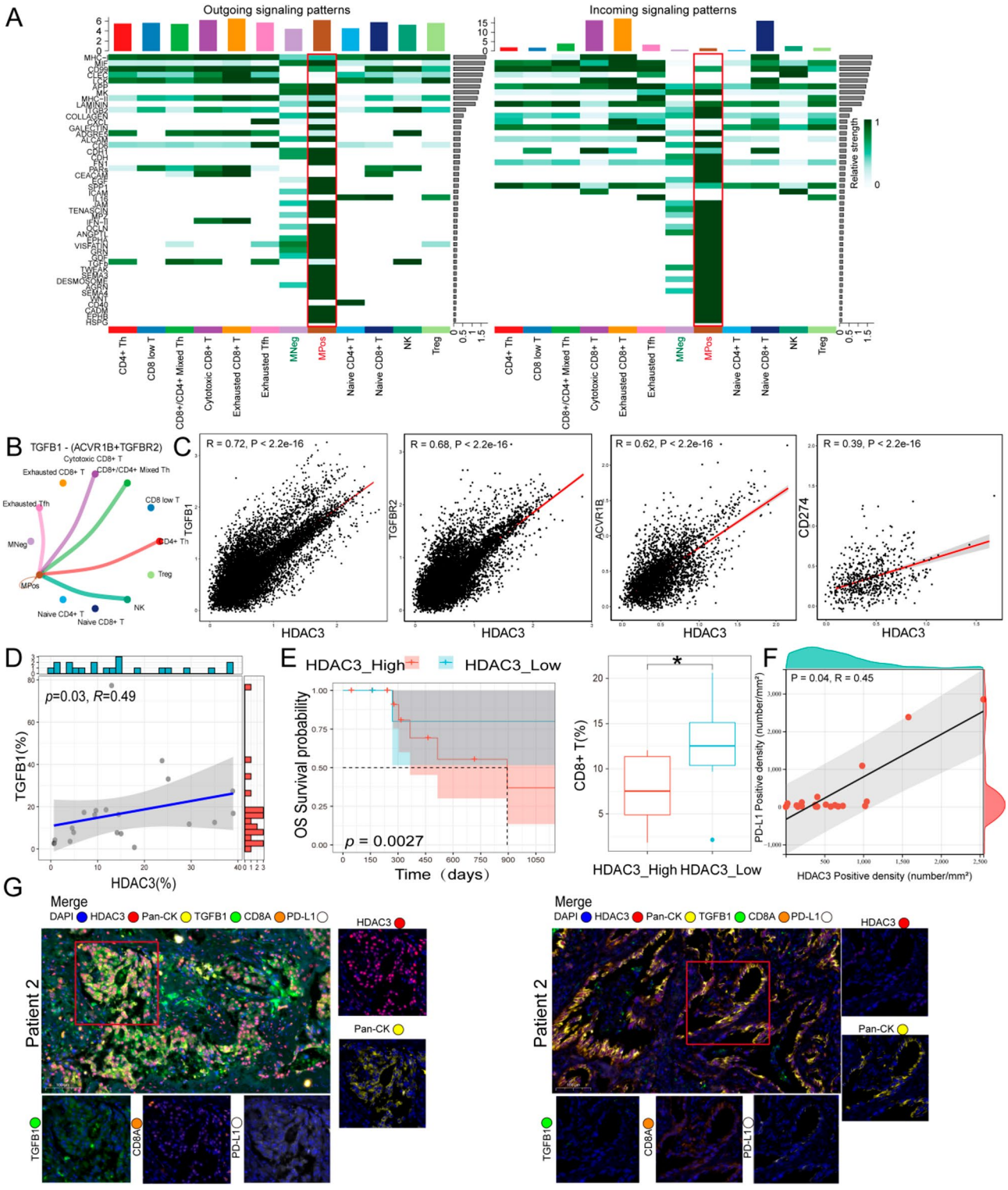

Fig. 5 Cell-Cell communications between *HDAC3*$^{+}$ and *HDAC3*$^{-}$ malignant cells and immune cells in single-cell RNA sequencing ($n=21$) and mIF cohort ($n=21$). **A**. Heatmap depicting the cell-cell communication network for both incoming and outgoing signaling analysis. **B**-**C**. Circular plots illustrating the quantity or intensity of interactions among various cell groups within the TGFB1-ACVR1B + TGFBR2 network, alongside correlations between *HDAC3* and *TGFB1*, *TGFBR2*, *ACVR1B*, and *CD274* between *HDAC3*$^{+}$ malignant cells and *HDAC3*$^{-}$ malignant cells. **D**. Correlation of TGFβ1^{+} percentage and HDAC3^{+} percentage. **E**. Kaplan-Meier analysis for OS based on HDAC3^{+} percentage and comparison of CD8^{+} T cell percentage in HDAC3 high and HDAC3 low groups. **F**. Correlation between PD-L1 and HDAC3 intensity. **G**. Representative mIF (20X) staining of HDAC3^{+} tumor cell, PD-L1, TGFβ1 and CD8^{+} T cells in patient #1 (OS = 48 days) and patient #2 (OS = 894 days). (Abbreviation: mIF: multiple immunofluorescence; OS: overall survival. * $p<0.05$.)

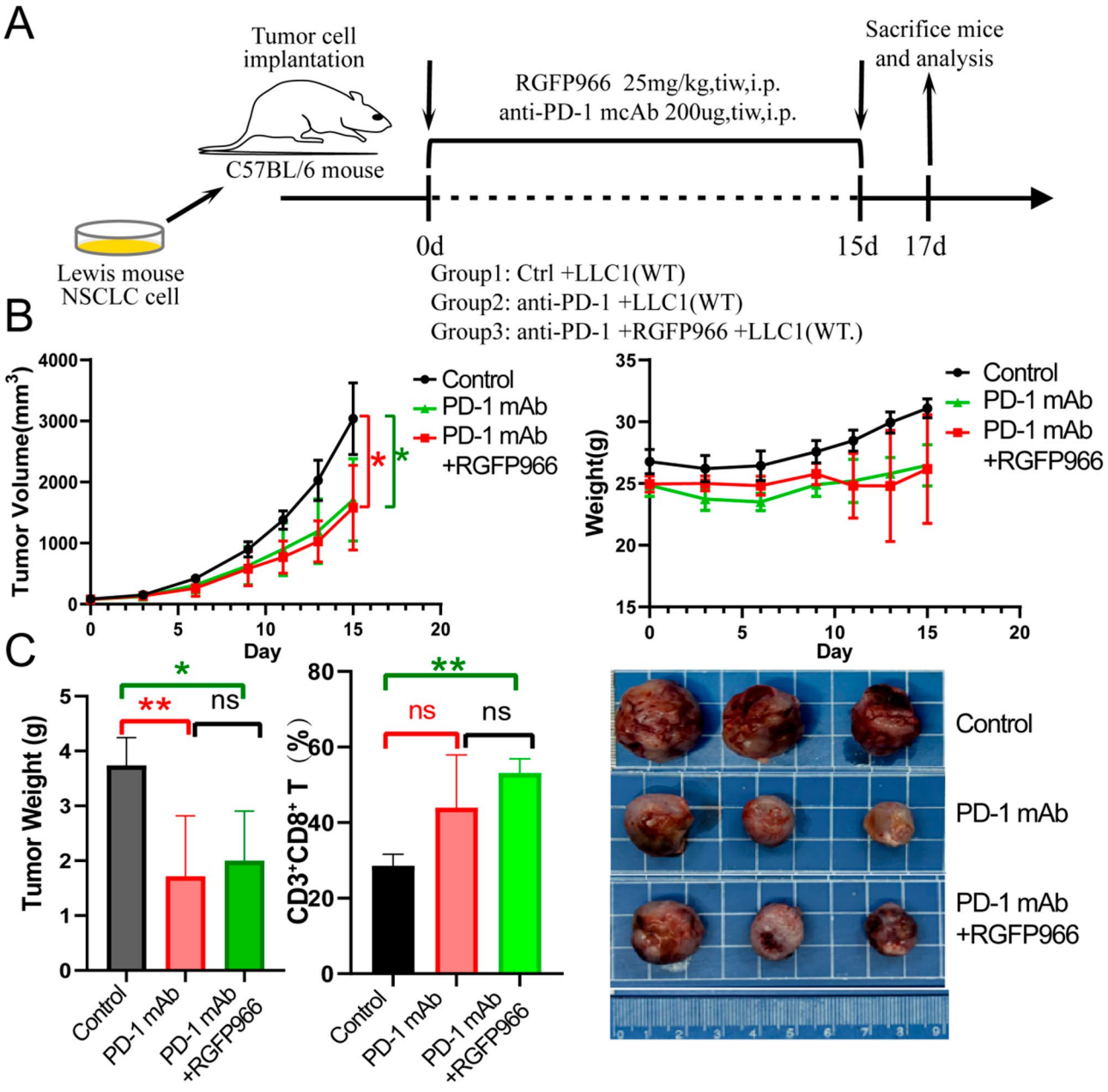

Fig. 6 HDAC3 inhibitor RGFP966 enhanced $CD8^+$ T cells infiltration in mouse model. **A**. Schematic protocol of the antitumor therapy using anti-PD-1 mAb and RGFP966 in C57BL/6 mice. **B**. Weight change curve and tumor growth curve of mice treated with PBS ($n=3$), anti-PD-1 mAb ($n=3$), or anti-PD-1 mAb plus RGFP966 ($n=3$). **C**. Weight of the harvested tumors ($n=3$) and quantification of the percent of $CD3^+$ $CD8^+$ T cells ($n=3$) in the tumors. (* $p<0.05$, ** $p<0.01$.)

to monotherapy, mice receiving combination treatment show slower tumor progression and higher survival rates. In pancreatic cancer, the specific HDAC3 inhibitor RGFP966 can reduce both PD-L1 protein and mRNA levels in pancreatic cancer cells [16]. In colorectal cancer, RGFP966 decreases PD-1^+ $CD8^+$ T cell infiltration in a dose-dependent manner [17]. In lymphoma, HDAC3 inhibitors have been shown to be more effective than pan-HDAC inhibitors, enhancing T cell activation against tumor cells [35]. RGFP966 can reverse abnormal epigenetic programming caused by CREBBP mutations [18] and affect lymphoma cells and the tumor microenvironment [35], upregulating PD-L1 expression in B-cell lymphoma [36], while restoring the ability of tumor-infiltrating lymphocytes to kill DLBCL cells, enhancing the effect of PD-L1 immunotherapy. In NSCLC, HDAC3 selective inhibitors combined with osimertinib have shown potential in treating *EGFR*-mutant non-small cell lung cancer, especially for polymorphisms with BIM deletions [45]. HDAC3 can inhibit T cell recruitment to

KRAS-mutant lung tumors, and combination therapy with KRAS pathway inhibitors and HDAC3 inhibitors can separate CXCL10 from immune-suppressive chemokines. The combination of entinostat and trametinib enhances in vivo T cell recruitment to lung tumors [49]. Furthermore, the combination of HDAC3-targeted drug entinostat with trametinib significantly inhibits tumor growth and overcomes resistance in *STK11*-mutant NSCLC [52]. Consistent with our research findings, high expression of HDAC3 and its antibodies is positively correlated with poor PFS and OS in NSCLC patients. Cellular and animal experiments suggest that HDAC3 is involved in regulating lung cancer cell proliferation and modulating $CD8^+$ T cell infiltration in vivo. Future research directions for HDAC3 inhibitors include (1) Development of highly selective inhibitors: Most current HDAC inhibitors (such as Entinostat [53]) exhibit some selectivity for HDAC3 but may still inhibit other Class I members such as HDAC1/2. Future efforts should focus on structural optimization or AI-based molecular design to develop inhibitors that specifically target HDAC3. (2) Deepening combination therapy strategies: HDAC3 inhibitors can enhance the sensitivity of other therapies through epigenetic regulation. This includes combination with targeted drugs [45], synergy with immunotherapy [50, 51], and the development of dual-target inhibitors. (3) Precision medicine and biomarker screening: Screening patient populations based on HDAC3 expression levels, specific gene mutations (such as *STK11* [52], *KRAS* [49] abnormalities), or epigenetic features can optimize treatment windows. Challenges in the future development of HDAC3 inhibitors include (1) Insufficient selectivity: Existing inhibitors may cross-inhibit other HDAC family subtypes (such as HDAC1/2), leading to off-target effects. Developing highly specific HDAC3 inhibitors will need to address the highly conserved nature of its catalytic domain. (2) Low clinical translation efficiency: Most HDAC3 inhibitors are still in preclinical or early clinical trial stages. Accelerating drug screening through organoid models or patient-derived xenograft platforms, and optimizing clinical trial designs (such as adaptive basket trials) to cover more tumor types, will be necessary. (3) Heterogeneity and resistance mechanisms cancers: Tumor cell heterogeneity and epigenetic plasticity may lead to adaptive resistance following HDAC3 inhibition. Multi-omics analyses are needed to uncover resistance mechanisms.

The future of HDAC3 inhibitors should focus on precision, combination, and technological innovation. By optimizing structure, guiding treatment with biomarkers, and upgrading delivery systems, current bottlenecks can be overcome. Additionally, a deeper understanding of the multidimensional regulatory network of HDAC3 in the tumor microenvironment will provide new insights to overcome resistance.

This study has several limitations. First, the small sample sizes may affect the generalizability and robustness of our findings. Larger, independent cohorts are necessary to validate these results, enhance statistical power, and improve reproducibility. Additionally, the study focuses on aNSCLC, limiting its applicability to other malignancies. The absence of key prognostic markers, such as PD-L1 expression and tumor mutational burden, restricts the ability to stratify analyses by PD-L1 status. Sufficient tumor tissue was not available for retrospective PD-L1 analysis in our AAb's cohorts. We acknowledge this limitation and plan to include PD-L1 assessment in future studies to further validate the relationship between HDAC3 and PD-L1 and its clinical significance in immunotherapy. Furthermore, further exploration of HDAC3's mechanisms is needed, and clinical trial validation of preclinical findings with RGFP966 and anti–PD-1 therapy is required.

Conclusion

In conclusion, our study underscores the importance of HDAC3 as a biomarker for predicting response to ICIs in aNSCLC and provides a rationale for further investigation into HDAC3-targeted therapies. Future studies should aim to explore the mechanisms by which HDAC3 influences TGFβ1 and $CD8^+$ T cells infiltration and the overall tumor microenvironment, paving the way for innovative strategies to improve immunotherapy outcomes.

Supplementary Information

The online version contains supplementary material available at https://doi.org/10.1186/s12931-025-03275-w.

Supplementary Material 1

Supplementary Material 2

Acknowledgements

Thanks to all the patients who participated in this study.

Author contributions

Liyuan Dai, Conceptualization, data curation, methodology, formal analysis, provided software, investigation, validation, visualization, writing—original draft, and writing—review & editing. Cuiling Zheng, Data curation, methodology, formal analysis, provided software, investigation, validation, visualization, and writing—review & editing. Liling Huang, Resources, data curation, investigation, and writing—review & editing. Lin Li, Resources, data curation, investigation, and writing—review & editing. Le Tang, Resources, data curation, investigation, and writing—review & editing. Jiarui Yao, Resources, data curation, investigation, and writing—review & editing.Yuankai Shi, Conceptualization, funding acquisition, supervision and writing—review & editing. Xiaohong Han, Conceptualization, funding acquisition, supervision and writing—review & editing. Liyuan Dai and Cuiling Zheng contributed equally to this work and as co-first authors.

Funding
This work was supported by the National High-Level Hospital Clinical Research Funding (2022-PUMCH-C-059), National High Level Hospital Clinical Research Funding (2022-PUMCH-B-033), CAMS Innovation Fund for Medical Sciences under Grant (CIFMS 2021-I2M-1-003), and the Major Project of Medical Oncology Key Foundation of Cancer Hospital Chinese Academy of Medical Sciences (CICAMS-MOMP2022006).

Data availability
No datasets were generated or analysed during the current study.

Declarations

Ethical approval
This study has been approved by the Ethics Committee of the National Cancer Center/National Clinical Research Center for Cancer/Cancer Hospital, Chinese Academy of Medical Sciences & Peking Union Medical College (No. 23/262–4004 and No.22/486–3688). All experiments were executed according to the Declaration of Helsinki.

Consent for publication
Not applicable.

Consent to participate
The experimental protocol was according to the ethical guidelines of the Helsinki Declaration and was approved by the Ethics Committee of the National Cancer Center/National Clinical Research Center for Cancer/Cancer Hospital, Chinese Academy of Medical Sciences & Peking Union Medical College (No. 23/262–4004 and No.22/486–3688).

Competing interests
The authors declare no competing interests.

Author details
[1]Department of Medical Oncology, Beijing Key Laboratory of Key Technologies for Early Clinical Trial Evaluation of Innovative Drugs for Major Diseases, National Cancer Center/National Clinical Research Center for Cancer/Cancer Hospital,Chinese Academy of Medical Sciences & Peking Union Medical College, No. 17 Panjiayuan Nanli, Chaoyang District, Beijing 100021, China
[2]Department of Pathology, National Cancer Center/National Clinical Research Center for Cancer/Cancer Hospital, Chinese Academy of Medical Sciences & Peking Union Medical College, No. 17 Panjiayuan Nanli, Chaoyang District, Beijing 100021, China
[3]Clinical Pharmacology Research Center,NMPA Key Laboratory for Clinical Research and Evaluation of Drug, Beijing Key Laboratory of Key Technologies for Early Clinical Trial Evaluation of Innovative Drugs for Major Diseases, Peking Union Medical College Hospital,Chinese Academy of Medical Sciences & Peking Union Medical College, No.1, Shuaifuyuan, Dongcheng District, Beijing 100730, China

Received: 30 October 2024 / Accepted: 14 May 2025
Published online: 12 June 2025

References

1. Sung H, Ferlay J, Siegel RL, et al. Global Cancer statistics 2020: GLOBOCAN estimates of incidence and mortality worldwide for 36 cancers in 185 countries. CA Cancer J Clin. 2021;71:209–49. https://doi.org/10.3322/caac.21660.
2. Gridelli C, Rossi A, Carbone DP, et al. Non-small-cell lung cancer. Nat Rev Dis Primers. 2015;1:15009. https://doi.org/10.1038/nrdp.2015.9.
3. Siegel RL, Giaquinto AN, Jemal Cancer A. statistics, 2024, CA Cancer J Clin, 74 (2024) 12–49. https://doi.org/10.3322/caac.21820
4. Xu S, Lu Exploring Z. FNDC4 as a biomarker for prognosis and immunotherapy response in lung adenocarcinoma. Asian J Surg. 2024. https://doi.org/10.1016/j.asjsur.2024.09.054.
5. Borghaei H, Paz-Ares L, Horn L, et al. Nivolumab versus docetaxel in advanced nonsquamous Non-Small-Cell lung Cancer. N Engl J Med. 2015;373:1627–39. https://doi.org/10.1056/NEJMoa1507643.
6. Reck M, Rodríguez-Abreu D, Robinson AG, et al. Pembrolizumab versus chemotherapy for PD-L1-Positive Non-Small-Cell lung Cancer. N Engl J Med. 2016;375:1823–33. https://doi.org/10.1056/NEJMoa1606774.
7. Bondarev AD, Attwood MM, Jonsson J, et al. Recent developments of HDAC inhibitors: emerging indications and novel molecules. Br J Clin Pharmacol. 2021;87:4577–97. https://doi.org/10.1111/bcp.14889.
8. Li J, Hu M, Liu N, et al. HDAC3 deteriorates colorectal cancer progression via microRNA-296-3p/TGIF1/TGFβ axis. J Exp Clin Cancer Res. 2020;39:248. https://doi.org/10.1186/s13046-020-01720-w.
9. Adhikari N, Amin SA, Trivedi P, et al. HDAC3 is a potential validated target for cancer: an overview on the benzamide-based selective HDAC3 inhibitors through comparative SAR/QSAR/QAAR approaches. Eur J Med Chem. 2018;157:1127–42. https://doi.org/10.1016/j.ejmech.2018.08.081.
10. Chen G, Yan Q, Liu L, et al. Histone deacetylase 3 governs β-Estradiol-ERα-Involved endometrial tumorigenesis via Inhibition of STING transcription. Cancers (Basel). 2022;14. https://doi.org/10.3390/cancers14194718.
11. Wu SM, Jan YJ, Tsai SC, et al. Targeting histone deacetylase-3 blocked epithelial-mesenchymal plasticity and metastatic dissemination in gastric cancer. Cell Biol Toxicol. 2023;39:1873–96. https://doi.org/10.1007/s10565-021-09673-2.
12. Minamiya Y, Ono T, Saito H, et al. Strong expression of HDAC3 correlates with a poor prognosis in patients with adenocarcinoma of the lung. Tumour Biol. 2010;31:533–9. https://doi.org/10.1007/s13277-010-0066-0.
13. Zhang J, Li J, Hou Y, et al. Osr2 functions as a Biomechanical checkpoint to aggravate CD8(+) T cell exhaustion in tumor. Cell. 2024;187:3409–e34263424. https://doi.org/10.1016/j.cell.2024.04.023.
14. Dent P, Booth L, Roberts JL, et al. (Curcumin + sildenafil) enhances the efficacy of 5FU and anti-PD1 therapies in vivo. J Cell Physiol. 2020;235:6862–74. https://doi.org/10.1002/jcp.29580.
15. Tay RE, Olawoyin O, Cejas P, et al. Hdac3 is an epigenetic inhibitor of the cytotoxicity program in CD8 T cells. J Exp Med. 2020;217. https://doi.org/10.1084/jem.20191453.
16. Hu G, He N, Cai C, et al. HDAC3 modulates cancer immunity via increasing PD-L1 expression in pancreatic cancer. Pancreatology. 2019;19:383–9. https://doi.org/10.1016/j.pan.2019.01.011.
17. Wang X, Fang Y, Liang W, et al. Fusobacterium nucleatum facilitates anti-PD-1 therapy in microsatellite stable colorectal cancer. Cancer Cell. 2024. https://doi.org/10.1016/j.ccell.2024.08.019.
18. Serganova I, Chakraborty S, Yamshon S, et al. Epigenetic, metabolic, and immune crosstalk in Germinal-Center-Derived B-Cell lymphomas: unveiling new vulnerabilities for rational combination therapies. Front Cell Dev Biol. 2021;9:805195. https://doi.org/10.3389/fcell.2021.805195.
19. Dai L, Tan Q, Li L, et al. High-Throughput antigen microarray identifies longitudinal prognostic autoantibody for chemoimmunotherapy in advanced Non-Small cell lung Cancer. Mol Cell Proteom. 2024;23:100749. https://doi.org/10.1016/j.mcpro.2024.100749.
20. Dai L, Chen H, Tan Q, et al. Identification of novel prognostic autoantibodies in diffuse large B-cell lymphoma treated with rituximab plus cyclophosphamide, doxorubicin, vincristine, and prednisone via a high-throughput antigen microarray. Cancer. 2024;130:1257–69. https://doi.org/10.1002/cncr.35158.
21. Kim N, Kim HK, Lee K, et al. Single-cell RNA sequencing demonstrates the molecular and cellular reprogramming of metastatic lung adenocarcinoma. Nat Commun. 2020;11:2285. https://doi.org/10.1038/s41467-020-16164-1.
22. Steen CB, Luca BA, Esfahani MS, et al. The landscape of tumor cell States and ecosystems in diffuse large B cell lymphoma. Cancer Cell. 2021;39:1422–e14371410. https://doi.org/10.1016/j.ccell.2021.08.011.
23. Kang J, Lee JH, Cha H, et al. Systematic dissection of tumor-normal single-cell ecosystems across a thousand tumors of 30 cancer types. Nat Commun. 2024;15:4067. https://doi.org/10.1038/s41467-024-48310-4.
24. Gautier L, Cope L, Bolstad BM, et al. affy–analysis of affymetrix genechip data at the probe level. Bioinformatics. 2004;20:307–15. https://doi.org/10.1093/bioinformatics/btg405.
25. Hao Y, Stuart T, Kowalski MH, et al. Dictionary learning for integrative, multimodal and scalable single-cell analysis. Nat Biotechnol. 2024;42:293–304. https://doi.org/10.1038/s41587-023-01767-y.
26. Patel AP, Tirosh I, Trombetta JJ, et al. Single-cell RNA-seq highlights intratumoral heterogeneity in primary glioblastoma. Science. 2014;344:1396–401. https://doi.org/10.1126/science.1254257.
27. Huber W, Carey VJ, Gentleman R, et al. Orchestrating high-throughput genomic analysis with bioconductor. Nat Methods. 2015;12:115–21. https://doi.org/10.1038/nmeth.3252.

28. Jin S, Guerrero-Juarez CF, Zhang L, et al. Inference and analysis of cell-cell communication using cellchat. Nat Commun. 2021;12:1088. https://doi.org/10.1038/s41467-021-21246-9.
29. Xu S, Chen X, Ying H, et al. Multi–omics identification of a signature based on malignant cell-associated ligand-receptor genes for lung adenocarcinoma. BMC Cancer. 2024;24:1138. https://doi.org/10.1186/s12885-024-12911-5.
30. Lu H, Ashiqueali R, Lin CI, et al. Histone deacetylase 3 Inhibition decreases cerebral edema and protects the Blood-Brain barrier after stroke. Mol Neurobiol. 2023;60:235–46. https://doi.org/10.1007/s12035-022-03083-z.
31. Xu C, Soragni E, Chou CJ, et al. Chemical probes identify a role for histone deacetylase 3 in Friedreich's ataxia gene Silencing. Chem Biol. 2009;16:980–9. https://doi.org/10.1016/j.chembiol.2009.07.010.
32. Robin X, Turck N, Hainard A, et al. pROC: an open-source package for R and S + to analyze and compare ROC curves. BMC Bioinformatics. 2011;12:77. https://doi.org/10.1186/1471-2105-12-77.
33. Sing T, Sander O, Beerenwinkel N, et al. ROCR: visualizing classifier performance in R. Bioinformatics. 2005;21:3940–1. https://doi.org/10.1093/bioinformatics/bti623.
34. Ogłuszka M, Orzechowska M, Jędroszka D, et al. Evaluate cutpoints: adaptable continuous data distribution system for determining survival in Kaplan-Meier estimator. Comput Methods Programs Biomed. 2019;177:133–9. https://doi.org/10.1016/j.cmpb.2019.05.023.
35. Mondello P, Tadros S, Teater M, et al. Selective Inhibition of HDAC3 targets synthetic vulnerabilities and activates immune surveillance in lymphoma. Cancer Discov. 2020;10:440–59. https://doi.org/10.1158/2159-8290.Cd-19-0116.
36. Deng S, Hu Q, Zhang H, et al. HDAC3 Inhibition upregulates PD-L1 expression in B-Cell lymphomas and augments the efficacy of Anti-PD-L1 therapy. Mol Cancer Ther. 2019;18:900–8. https://doi.org/10.1158/1535-7163.Mct-18-1068.
37. Dai L, Fan G, Xie T, et al. Single-cell and Spatial transcriptomics reveal a high Glycolysis B cell and tumor-associated macrophages cluster correlated with poor prognosis and exhausted immune microenvironment in diffuse large B-cell lymphoma. Biomark Res. 2024;12:58. https://doi.org/10.1186/s40364-024-00605-w.
38. Werbeck ND, Shukla VK, Kunze MBA, et al. A distal regulatory region of a class I human histone deacetylase. Nat Commun. 2020;11:3841. https://doi.org/10.1038/s41467-020-17610-w.
39. Bhaskara S, Chyla BJ, Amann JM, et al. Deletion of histone deacetylase 3 reveals critical roles in S phase progression and DNA damage control. Mol Cell. 2008;30:61–72. https://doi.org/10.1016/j.molcel.2008.02.030.
40. Fang C, Wang Y, Li Y. [Research progress of histone deacetylase inhibitor combined with immune checkpoint inhibitor in the treatment of tumor]. Zhongguo Fei Ai Za Zhi. 2021;24:204–11. https://doi.org/10.3779/j.issn.1009-3419.2021.102.11.
41. Peng Z, Zhou W, Zhang C, et al. Curcumol controls choriocarcinoma Stem-Like cells Self-Renewal via repression of DNA methyltransferase (DNMT)- and histone deacetylase (HDAC)-Mediated epigenetic regulation. Med Sci Monit. 2018;24:461–72. https://doi.org/10.12659/msm.908430.
42. Hsieh HY, Chuang HC, Shen FH, et al. Targeting breast cancer stem cells by novel HDAC3-selective inhibitors. Eur J Med Chem. 2017;140:42–51. https://doi.org/10.1016/j.ejmech.2017.08.069.
43. Najjary S, de Koning W, Kros JM, et al. Unlocking molecular mechanisms and identifying druggable targets in matched-paired brain metastasis of breast and lung cancers. Front Immunol. 2023;14:1305644. https://doi.org/10.3389/fimmu.2023.1305644.
44. Lou T, Liu C, Qu H, et al. FOXA1 can be modulated by HDAC3 in the progression of epithelial ovarian carcinoma. J Transl Med. 2022;20:19. https://doi.org/10.1186/s12967-021-03224-3.
45. Tanimoto A, Takeuchi S, Arai S, et al. Histone deacetylase 3 Inhibition overcomes BIM deletion Polymorphism-Mediated osimertinib resistance in EGFR-Mutant lung Cancer. Clin Cancer Res. 2017;23:3139–49. https://doi.org/10.1158/1078-0432.Ccr-16-2271.
46. Liu D, Wei B, Liang L, et al. The circadian clock component RORA increases immunosurveillance in melanoma by inhibiting PD-L1 expression. Cancer Res. 2024;84:2265–81. https://doi.org/10.1158/0008-5472.Can-23-3942.
47. Wei X, Liu J, Cheng J, et al. Super-enhancer-driven ZFP36L1 promotes PD-L1 expression in infiltrative gastric cancer. Elife. 2024;13. https://doi.org/10.7554/eLife.96445.
48. Stergiou IE, Palamaris K, Levidou G et al. PD-L1 Expression in Neoplastic and Immune Cells of Thymic Epithelial Tumors: Correlations with Disease Characteristics and HDAC Expression, Biomedicines, 12 (2024) https://doi.org/10.3390/biomedicines12040772
49. Li L, Hao S, Gao M, et al. HDAC3 Inhibition promotes antitumor immunity by enhancing CXCL10-Mediated chemotaxis and recruiting of immune cells. Cancer Immunol Res. 2023;11:657–73. https://doi.org/10.1158/2326-6066.Cir-22-0317.
50. Woods DM, Sodré AL, Villagra A, et al. HDAC Inhibition upregulates PD-1 ligands in melanoma and augments immunotherapy with PD-1 Blockade. Cancer Immunol Res. 2015;3:1375–85. https://doi.org/10.1158/2326-6066.Cir-15-0077-t.
51. Terranova-Barberio M, Thomas S, Ali N, et al. HDAC Inhibition potentiates immunotherapy in triple negative breast cancer. Oncotarget. 2017;8:114156–72. https://doi.org/10.18632/oncotarget.23169.
52. Eichner LJ, Curtis SD, Brun SN, et al. HDAC3 is critical in tumor development and therapeutic resistance in Kras-mutant non-small cell lung cancer. Sci Adv. 2023;9:eadd3243. https://doi.org/10.1126/sciadv.add3243.
53. Trapani D, Esposito A, Criscitiello C, et al. Entinostat for the treatment of breast cancer. Expert Opin Investig Drugs. 2017;26:965–71. https://doi.org/10.1080/13543784.2017.1353077.

Publisher's note